INTERNATIONAL JOURNAL FOR NUMERICAL METHODS IN FLUIDS
Int. J. Numer. Meth. Fluids 2005; **49**:763–783
Published online 24 June 2005 in Wiley InterScience (www.interscience.wiley.com). DOI: 10.1002/fld.1030

Finite volume solution to integrated shallow surface–saturated groundwater flow

K. S. Erduran[1,*,†], V. Kutija[1,‡] and C. R. Macalister[2]

[1] *WRSRL, Cassie Building, Department of Civil Engineering, University of Newcastle upon Tyne NE1 7RU, U.K.*
[2] *CLUWRR, Porter Building, University of Newcastle upon Tyne NE1 7RU, U.K.*

SUMMARY

This paper describes development of an integrated shallow surface and saturated groundwater model (GSHAW5). The surface flow motion is described by the 2-D shallow water equations and groundwater movement is described by the 2-D groundwater equations. The numerical solution of these equations is based on the finite volume method where the surface water fluxes are estimated using the Roe shock-capturing scheme, and the groundwater fluxes are computed by application of Darcy's law. Use of a shock-capturing scheme ensures ability to simulate steady and unsteady, continuous and discontinuous, subcritical and supercritical surface water flow conditions. Ground and surface water interaction is achieved by the introduction of source-sink terms into the continuity equations. Two solutions are tightly coupled in a single code. The numerical solutions and coupling algorithms are explained. The model has been applied to 1-D and 2-D test scenarios. The results have shown that the model can produce very accurate results and can be used for simulation of situations involving interaction between shallow surface and saturated groundwater flows. Copyright © 2005 John Wiley & Sons, Ltd.

KEY WORDS: shallow water equations; saturated groundwater equation; finite volume; shock-capturing scheme; surface and groundwater coupling

1. INTRODUCTION

In nature, surface water often interacts with groundwater and they exchange flow. Such a flow interaction can often be observed between rivers and aquifers and in and around wetlands

*Correspondence to: K. S. Erduran, Hydraulic Division, Civil Engineering Department, University of Nigde, 51100 Nigde, Turkey.
†E-mail: kserduran@nigde.edu.tr, kerduran@hotmail.com
‡E-mail: vedrana.kutija@ncl.ac.uk

Contract/grant sponsor: Ministry of Education of Turkey
Contract/grant sponsor: University of Newcastle Ridley Fellowship Fund

Received 11 July 2003
Revised 4 February 2005
Accepted 17 May 2005

where overland flows interact with aquifer flows. These interactive flow processes have been experimentally and numerically studied for many years for several reasons such as groundwater contamination analysis and wetland management.

These studies have led to the development of many integrated groundwater (GW) and surface water (SW) numerical models. Two main characteristics help us to distinguish these models: the type of equations and the solution methods used as well as the type of coupling. Surface water flow processes are generally described by two-dimensional (2-D) shallow water equations or 1-D de Saint-Venant equations. Further simplified equations such as diffusion or kinematic wave equations are also employed for the overland flow. Groundwater flow is modelled by solving either Richards equation (saturated, unsaturated and variable-saturated flow), or a rather simple equation, which is based on Darcy's law and only suitable for simulation of saturated flow processes [1–3]. The degree of complexity also depends on the spatial dimension used, i.e. (1-D, 2-D or 3-D models), and whether the flow has a time dimension (unsteady or not). One can also distinguish two types of coupling; external (loose) coupling and internal (tight) coupling [4]. In external coupling, surface and groundwater simulation is carried out one after another whereas in internally coupled models coupling is provided within the same time level. The latter requires a single source written for both surface and groundwater computations and this coupling is also rather more difficult to implement compared with external coupling.

GSHAW5 (Groundwater and SHAllow Water equations solved by FInite VolumE method) is an integrated 2-D ground and surface water model, developed at Newcastle University. Solution of the 2-D shallow water equations and 2-D groundwater equation is achieved by the finite volume method (FVM). The FVM is based on integration of the equations of interest over each finite volume (cell) covering the computational domain. The key element in FVM is to estimate the fluxes at cell interfaces. In the surface water calculation, fluxes through the cell interfaces are computed using the Roe scheme [5]. The solution to surface water equations by the FVM and Roe scheme is suitable for many types of flows including continuous to discontinuous flow, subcritical to supercritical and steady to unsteady flow. It is also capable of simulating drying and wetting processes. In the literature, examples can be found where Roe scheme has been very successfully applied to severe flow conditions such as simulation of dam break and oblique shock problems [6, 7]. Many other similar models are based on finite difference schemes and have difficulty simulating supercritical and transcritical flows as well as phenomena of drying and wetting of the land to a reasonable degree of accuracy [8]. To avoid these problems, the authors have opted for the FVM with a shock-capturing scheme for the surface component of the model. Numerical solution of the groundwater equation uses the same cells as the solution of the surface flow equations. However, in the groundwater solution fluxes through cell interfaces are calculated according to Darcy's law. Integration is achieved by the introduction of source-sink terms in the continuity equations of both ground and surface water solutions. These source-sink terms include leakage from surface to subsurface and a flow from the subsurface to surface. Additionally, in some cases, compatibility of groundwater head and surface water level is maintained.

Solution of the 2-D groundwater equation is described in Section 2 and the solution to 2-D shallow water equations is given in Section 3. The coupling processes are explained in Section 4. The features of the model are briefly given in Section 5. Section 6 illustrates test scenarios and the results. Finally, conclusions are drawn and outlined in Section 7.

2. SOLUTION TO GROUNDWATER EQUATIONS

The 2-D groundwater flow equation for homogeneous fluid with constant density can be given [9, 10] as

$$S_y \frac{\partial H}{\partial t} = \frac{\partial}{\partial x}\left(K_x E \frac{\partial H}{\partial x}\right) + \frac{\partial}{\partial y}\left(K_y E \frac{\partial H}{\partial y}\right) \tag{1}$$

where S_y is the specific yield, H is the groundwater head, K_x and K_y are the hydraulic conductivity in x and y directions, respectively, and E is the thickness of fully saturated groundwater inside the aquifer.

Equation (1) is known as the continuity (mass balance) equation for 2-D groundwater flow in porous media and is also known as the nonlinear Boussinesq equation [10]. The groundwater equation can also be written as

$$\begin{gathered} S_y \frac{\partial H}{\partial t} = \frac{\partial f_x}{\partial x} + \frac{\partial f_y}{\partial y} = \nabla \cdot \mathbf{F} \\ \mathbf{F} = [f_x, f_y] \end{gathered} \tag{2}$$

where $\nabla\cdot$ is a divergence operator and f_x and f_y are the fluxes (specific discharges) in x and y direction, respectively, and they can be denoted as

$$f_x = K_x E \frac{\partial H}{\partial x}, \quad f_y = K_y E \frac{\partial H}{\partial y} \tag{3}$$

In the FVM the domain is divided into disjunctive subdomains called cells (Figure 1) and the solution is based on the integration of equations over these cells. Application of divergence theorem to the flux term and integration of Equation (2) over a control volume V results in

$$\int_V \left(S_y \frac{\partial H}{\partial t}\right) \mathrm{d}V = \int_V (\operatorname{div} \mathbf{F})\, \mathrm{d}V = \int_S (\mathbf{F} \cdot \mathbf{n})\, \mathrm{d}S = \oint_L f_x\, \mathrm{d}y - f_y\, \mathrm{d}x \tag{4}$$

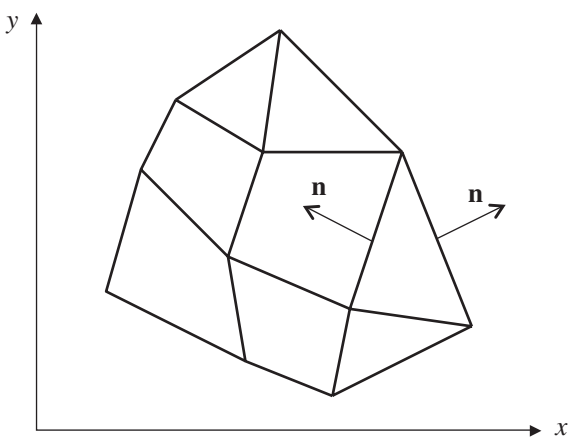

Figure 1. Typical finite volume cell and outward normal vector, **n**.

where **n** is an outward normal vector, S denotes the surface integral, and L represents the line integral. This method is applicable to unstructured and non-uniform grids if the hydraulic conductivity values are provided for all outward normal vector directions at every cell interfaces. Further in this paper, the detail of the solution will be presented for the rectangular grid only. Hence, for a rectangular cell (Figure 2), the discrete form of the above relation can be written as follows:

$$A_c S_y \frac{\partial H}{\partial t} = f_{x1}(y_B - y_A) - f_{y1}(x_B - x_A) + f_{x2}(y_C - y_B) - f_{y2}(x_C - x_B) + f_{x3}(y_D - y_C) - f_{y3}(x_D - x_C) + f_{x4}(y_A - y_D) - f_{y4}(x_A - x_D)$$

where A_c is the area of the cell, x_A, x_B, x_C, x_D are x co-ordinate of points A, B, C, D, respectively, similarly y_A, y_B, y_C, y_D are y co-ordinate of points A, B, C, D, respectively, subscripts 1, 2, 3, 4 refer to the side of the cell as shown in Figure 2. Finally, Equation (2) may be rewritten as

$$A_c S_y \frac{\partial H}{\partial t} = \sum_{j=1}^{k} \mathbf{f}_j L_j \tag{5}$$

where k is the number of sides of a cell.

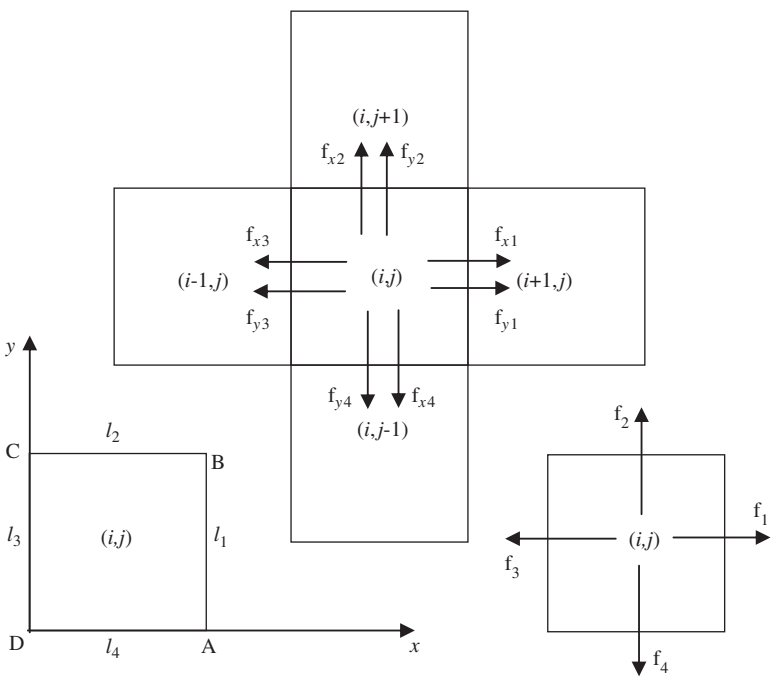

Figure 2. Cell interface groundwater fluxes and integration paths.

2.1. Estimation of the fluxes by Darcy's law

The key element in the FVM is the computation of the fluxes through cell interfaces. They can be computed by Darcy's law for each direction (Figure 2).

For instance, flux through the interface $(i+1/2, j)$ can be given in discretized form as

$$f_1 = K_{x(i+1/2,j)} \frac{(H_{i+1,j} - H_{i,j})}{\mathrm{abs}(X_{i,j} - X_{i+1,j})} E_{(i+1/2,j)} \tag{6}$$

where $E_{(i+1/2,j)} = (H_{i,j} + H_{i+1,j}/2)$ if groundwater head is under the ground level, $H < Z$. $E_{(i+1/2,j)} = (Z_{i,j} + Z_{i+1,j}/2)$ if groundwater head is above the ground level, $H > Z$, where Z is the vertical distance at the centre of the cell measured from datum to the ground surface (so it is also the thickness of the aquifer); similarly, X is the x co-ordinate of the centre of the cell. In the same way, remaining fluxes for the other interfaces can be computed.

Finally, the solution for H can be obtained from Equation (5) by Euler time integration

$$H^{\mathrm{up}} = H^n + \frac{\Delta t}{A_c S_y} \sum_{j=1}^{k} \mathbf{f}_j L_j \tag{7}$$

where n is the present time step, and H^{up} is a solution for H over a time step Δt.

However, solution of Equation (7) may not be the final solution for H as it will be explained at the end of Section 4. Hence, the notation H^{up} instead of H^{n+1} is used ($n+1$ stands for the next time step).

3. SOLUTION TO SHALLOW WATER EQUATIONS

The 2-D form of the shallow water equations can be written as:

$$\begin{aligned}
&\frac{\partial h}{\partial t} + \frac{\partial (h v_x)}{\partial x} + \frac{\partial (h v_y)}{\partial y} = 0 \\
&\frac{\partial (h v_x)}{\partial t} + \frac{\partial (h v_x^2 + g h^2/2)}{\partial x} + \frac{\partial (h v_x v_y)}{\partial y} = g h (So_x - Sf_x) \\
&\frac{\partial (h v_y)}{\partial t} + \frac{\partial (h v_x v_y)}{\partial x} + \frac{\partial (h v_y^2 + g h^2/2)}{\partial y} = g h (So_y - Sf_y)
\end{aligned} \tag{8}$$

where h is the water depth, v_x, v_y represent the depth-averaged velocity components in the x and y directions, respectively, g is the acceleration due to gravity, So_x and Sf_x are the bed slope and friction terms, respectively, in the x direction and, similarly, So_y and Sf_y are the bed slope and friction terms, respectively, in the y direction.

Denoting $p_1 = h$, $p_2 = h v_x$, $p_3 = h v_y$ and defining the conserved physical vector $\mathbf{p} = [p_1, p_2, p_3]^{\mathrm{T}}$, the conservative vector form of the shallow water equations can be written in vector notation as

$$\frac{\partial \mathbf{p}}{\partial t} + \frac{\partial \mathbf{f}(\mathbf{p})}{\partial x} + \frac{\partial \mathbf{g}(\mathbf{p})}{\partial y} = \mathbf{b}(\mathbf{p}) \tag{9}$$

where $\mathbf{f}(\mathbf{p})$, $\mathbf{g}(\mathbf{p})$ are the flux vectors in the x, y directions, respectively, and $\mathbf{b}(\mathbf{p})$ denotes source/sink terms.

Equation (9) can also be written in the compact-conservative form given below by denoting $\mathbf{F}(\mathbf{p}) = [\mathbf{f}(\mathbf{p}), \mathbf{g}(\mathbf{p})]^{\mathrm{T}}$

$$\frac{\partial \mathbf{p}}{\partial t} + (\nabla \cdot \mathbf{F})^{\mathrm{T}} = \mathbf{b}(\mathbf{p}) \tag{10}$$

The FVM is based on integration of the equations of interest over each finite volume (cell) covering the computational domain. Thus,

$$\int_V \left(\frac{\partial \mathbf{p}}{\partial t} + (\nabla \cdot \mathbf{F})^{\mathrm{T}} \right) \mathrm{d}V = \int_V \mathbf{b}(\mathbf{p}) \, \mathrm{d}V \tag{11}$$

where V represents the volume over which integration is performed.

Assuming that $\mathbf{p}$ varies with time but is constant over the cell, applying the divergence theorem to the second term on the left-hand side of Equation (11), using the rotational invariance property between $\mathbf{f}(\mathbf{p})$ and $\mathbf{g}(\mathbf{p})$ on each side of the cell and resolving $\mathbf{F}(\mathbf{p})$ in the direction of the normal vector $\mathbf{n}$, the 2-D equations are reduced to a number of 1-D local Riemann problems [6] which are solved separately; one across each cell boundary. In discretized form these are given by

$$A_{\mathrm{c}} \frac{\mathrm{d}\mathbf{p}}{\mathrm{d}t} = -\sum_{k=1}^{m} \mathbf{T}^{-1}(\theta^k) \mathbf{f}^k(\mathbf{q}^k) L^k + \int_V \mathbf{b}(\mathbf{p}) \, \mathrm{d}V \tag{12}$$

where A_{c} is the area of the cell, m is the number of sides of the cell, k is an index that represents the side of a cell, L^k is the length of the kth cell side, θ^k is the angle between the outward normal vector $\mathbf{n}$ and the x-axis, $\mathbf{T}(\theta^k)$ is the transformation matrix which can be obtained by rotating the co-ordinate axes, $\mathbf{T}^{-1}(\theta^k)$ is the inverse transformation matrix, $\mathbf{q}^k$ is the transformed conserved physical vector obtained by multiplying $\mathbf{p}$ by the transformation matrix and $\mathbf{f}^k(\mathbf{q}^k)$ is the transformed numerical flux vector. We have

$$\mathbf{q} = -\mathbf{T}(\theta)\mathbf{p} = [h, hu, hv]^{\mathrm{T}}, \quad \mathbf{f}(\mathbf{q}) = [hu, hu^2 + gh^2/2, huv]^{\mathrm{T}}$$

$$\mathbf{T}(\theta) = \begin{bmatrix} 1 & 0 & 0 \\ 0 & \cos\theta & \sin\theta \\ 0 & -\sin\theta & \cos\theta \end{bmatrix} \quad \text{and} \quad \mathbf{T}^{-1}(\theta) = \begin{bmatrix} 1 & 0 & 0 \\ 0 & \cos\theta & -\sin\theta \\ 0 & \sin\theta & \cos\theta \end{bmatrix}$$

where u, v are local components of velocity in the normal and tangential directions to the cell boundary, respectively, given by

$$u = v_x \cos\theta + v_y \sin\theta, \quad v = -v_x \sin\theta + v_y \cos\theta$$

If we let x^n be a local co-ordinate, normal to the cell side, the Riemann problem can be written as

$$\frac{\partial \mathbf{q}}{\partial t} + \frac{\partial \mathbf{f}(\mathbf{q})}{\partial x^n} = \mathbf{0} \tag{13}$$

The initial state is given by

$$\mathbf{q}(x^n, 0) = \begin{cases} \mathbf{q}_{\mathrm{L}}; & x^n < 0 \\ \mathbf{q}_{\mathrm{R}}; & x^n > 0 \end{cases}$$

where $\mathbf{q}_L$ and $\mathbf{q}_R$ denote the values of the transformed conserved physical vector to the left and right of the cell interface, respectively. The inside of the cell under consideration always corresponds to the left-hand side of the Riemann interface, and the neighbouring cell to the right-hand side.

Equation (13) is solved by the Roe scheme [5], giving the numerical fluxes through each cell interface. The overall finite volume solution to the shallow water equations and the estimation of the numerical fluxes using the Roe scheme can be found in detail in many references [6, 7, 11–16] and it will not be replicated in this paper to avoid repetition.

The upwinding technique [14, 17, 18] is applied to the treatment of the bottom slope in order to achieve the accurate flux balance. Following these references, first the source and sink terms are separated as follows.

$\mathbf{b} = \mathbf{b}^1 + \mathbf{b}^2$ where $\mathbf{b}^1$ denotes the source term (bottom slope) and $\mathbf{b}^2$ denotes sink term (friction). Then, the source term is replaced by the discrete numerical source term as shown below:

$$\tilde{\mathbf{b}}_k^1 = \frac{1}{2}\sum_{i=1}^{3} \beta^{i-}\tilde{\gamma}^i \tag{14}$$

where $\tilde{\mathbf{b}}_k^1$ is the numerical source term, written for every cell interface k, and

$$\beta^{1-} = \frac{-1}{2\tilde{c}}\left(1 - \frac{|\tilde{\lambda}_1|}{\tilde{\lambda}_1}\right)[g\tilde{h}\Delta z_x \cos\theta + g\tilde{h}\Delta z_y \sin\theta]$$

$$\beta^{2-} = \left(1 - \frac{|\tilde{\lambda}_2|}{\tilde{\lambda}_2}\right)[-g\tilde{h}\Delta z_x \sin\theta + g\tilde{h}\Delta z_y \cos\theta]$$

$$\beta^{3-} = \frac{-1}{2\tilde{c}}\left(1 - \frac{|\tilde{\lambda}_3|}{\tilde{\lambda}_3}\right)[g\tilde{h}\Delta z_x \cos\theta + g\tilde{h}\Delta z_y \sin\theta]$$

$$\tilde{\gamma}^1 = [1, \tilde{u} - \tilde{c}, \tilde{v}]^T, \quad \tilde{\gamma}^2 = [0, 0, 1]^T, \quad \tilde{\gamma}^3 = [1, \tilde{u} + \tilde{c}, \tilde{v}]^T, \quad \tilde{\lambda}_1 = \tilde{u} - \tilde{c}, \quad \tilde{\lambda}_2 = \tilde{u}, \quad \tilde{\lambda}_3 = \tilde{u} + \tilde{c}$$

$\Delta z_x = -(z_R - z_L)\cos\theta$, $\Delta z_y = -(z_R - z_L)\sin\theta$. Roe-averaged quantities are given as

$$\tilde{h} = \frac{h_L + h_R}{2}, \quad \tilde{c} = \sqrt{\frac{g(h_L + h_R)}{2}}, \quad \tilde{u} = \frac{h_R^{1/2}u_R + h_L^{1/2}u_L}{h_R^{1/2} + h_L^{1/2}} \quad \text{and} \quad \tilde{v} = \frac{h_R^{1/2}v_R + h_L^{1/2}v_L}{h_R^{1/2} + h_L^{1/2}}$$

The source term can be written as follows:

$$\int_V \mathbf{b}^1 \, \mathrm{d}V = \sum_{k=1}^{m} \mathbf{T}^{-1}(\theta^k)\tilde{\mathbf{b}}_k^1 L^k \tag{15}$$

Hence, Equation (12) can be rewritten as

$$\mathbf{p}^{n+1} = \mathbf{p}^n - \frac{\Delta t}{A_c} \sum_{k=1}^{m} [\mathbf{f}^k(\mathbf{q}^k) - \tilde{\mathbf{b}}_k^1]\mathbf{T}^{-1}(\theta^k)L^k + \Delta t \mathbf{b}_2 \tag{16}$$

where $\mathbf{p}^{n+1}$ shows values at the next time step, Δt is the length of the time step and

$$\mathbf{b}_2 = [0, Sf_x, Sf_y]^T, \quad Sf_x = \frac{n^2 v_x \sqrt{v_x^2 + v_y^2}}{h^{4/3}}, \quad Sf_y = \frac{n^2 v_y \sqrt{v_x^2 + v_y^2}}{h^{4/3}}$$

Equation (16) is applied to every finite volume cell.

3.1. Inclusion of rainfall

Rainfall can also be simulated in GSHAW5 by introducing rainfall intensity as a source term in the continuity equation of the shallow water equations. The solution is achieved using the splitting technique [12].

$$\frac{\partial h}{\partial t} + \frac{\partial (h v_x)}{\partial x} + \frac{\partial (h v_y)}{\partial y} = q_R \tag{17}$$

where q_R is rainfall intensity (m/s). Splitting the continuity equations as

$$\frac{\partial h}{\partial t} = q_R \tag{18}$$

and

$$\frac{\partial h}{\partial t} + \frac{\partial (h v_x)}{\partial x} + \frac{\partial (h v_y)}{\partial y} = 0$$

Equation (18) is an ODE (ordinary differential equation) and can be solved by a simple Euler method given below.

$$h^{up} = h + \Delta t q_R \tag{19}$$

where h^{up} illustrates the solution to h over a time step Δt due to the source term (rainfall) only.

Since solution of Equation (19) is not the final solution for h, the notation h^{up} (for h updated) instead of h^{n+1} is used (see Section 4 for more details).

Finally, the overall solution including the rainfall effect can be achieved in two steps:

Step 1: Use Equation (19) to update the first component of **P**, h.
Step 2: Use Equation (16) to find the next time step values for all three components of **P**.

4. COUPLING SURFACE WATER WITH GROUNDWATER

Figure 3 shows the coupling processes used in GSHAW5. There are three cases implemented in the model:

Case A: The surface is wet and the water depth is prescribed, but the groundwater head is below the ground level elevation for that cell. In this case, there will be a flow from surface to ground due to leakage, computed by Darcy's law in the z direction:

$$q_i = K_z(h + Z - H)/Z \tag{20}$$

where q_i is the flow due to infiltration, K_z is a hydraulic conductivity in z direction. The similar expression for the computation of leakage can be found in Wilson and Akande [19], and Haagsma and Johanns [4].

Infiltration results in increasing groundwater head and decreasing surface water depth. Hence, q_i is introduced as a source term to groundwater and sink term to surface water continuity equations. Then, the splitting technique is applied to each continuity equation. Each application then produces an ODE, which is solved by the first order Euler method. For instance, introducing q_i as a source term to Equation (1) gives

$$S_y \frac{\partial H}{\partial t} = \frac{\partial}{\partial x}\left(K_x E \frac{\partial H}{\partial x}\right) + \frac{\partial}{\partial y}\left(K_y E \frac{\partial H}{\partial y}\right) + q_i \tag{21}$$

Application of the splitting technique to Equation (21) yields two equations. The first is an ODE given in Equation (22). The second is Equation (1) given earlier.

$$S_y \frac{\partial H}{\partial t} = q_i \tag{22}$$

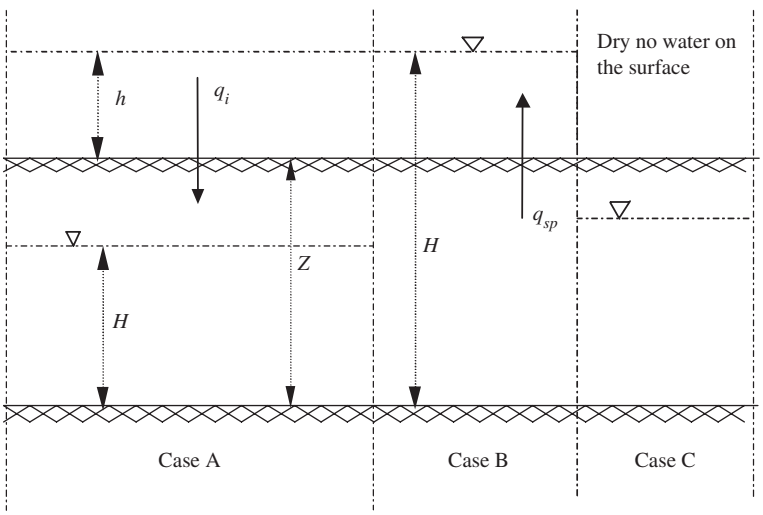

Figure 3. The coupling processes: Cases A, B and C.

By using the first order Euler method, the solution to Equation (22) is obtained.

$$H^{\mathrm{up}} = H^n + \frac{\Delta t q_i}{S_y} \tag{23}$$

Solution to Equation (1) is already given in Equation (7). Note that the updated groundwater head values obtained from Equation (23) are used as the present time step groundwater head values in Equation (7).

Similarly, resulting ODE for the surface water can be solved as

$$h^{\mathrm{up}} = h^n - \Delta t q_i \tag{24}$$

Lateral flow computation for the surface water is also carried out, using the updated water depth values obtained from Equation (24) as the present time step values in Equation (16).

Case B: The groundwater head is above the ground level and is equal to $h+Z$. The surface is wet and there is no infiltration. In this case, an interaction between groundwater and surface water is assured by compatibility of the groundwater head and the water level. Again, the surface water depth and groundwater head is recomputed by

(a) Equation (7), which takes into account the change in storage and gives a solution to H over a time step, Δt.
(b) Introducing another source term, q_{sp}, into the continuity equation of the shallow water equations.

$$q_{sp} = \frac{1}{A_{\mathrm{c}}} \sum_{j=1}^{k} \mathbf{f}_j L_j$$

Then, the splitting technique is applied and the solution is achieved as

$$h^{\mathrm{up}} = h^n + \frac{\Delta t}{A_{\mathrm{c}}} \sum_{j=1}^{k} \mathbf{f}_j L_j \tag{25}$$

q_{sp} is actually equal to the second term on the right-hand side of Equation (7). The only difference is that, here, S_y is omitted as the groundwater head is above the ground surface.
(c) When the surface water computation is complete and shallow water depth has changed, the groundwater head, given by the sum of h and Z, must be updated.

Case C: There is no water on the surface and the cells are effectively dry. To avoid the zero-division problem, water depth is the prescribed value 0.00001 m. There is no integration between ground and surface. However, Equations (7) and (16) are still applied in order to compute the changes due to the horizontal water movements in both ground and surface water.

Finally, the computation in GSHAW5 is carried out as follows:

(1) Flow due to rainfall: Equation (19) is used.
(2) Infiltration: Equations (23) and (24) are used.
(3) Groundwater flow computation: Equation (7) is used. If Case B occurs then Equation (25) is used.
(4) Surface water computation: Equation (16) is used. If Case B occurs then the groundwater head is recalculated.

The updated value of depth, h^{up}, is obtained from Equations (19), (24) and (25). The updated value of groundwater head, H^{up}, is obtained from Equations (7) and (23). If those equations are the final equations used according to the steps described above, then h^{up} and H^{up} become h^{n+1} and H^{n+1}, respectively. Otherwise, h^{up} and H^{up} are used as intermediate values, denoted by h^n and H^n, respectively in the following equations. For instance, in Case A, when some rain occurs, the next time step value (h^{n+1}) for h is obtained from the solution to Equation (16) not the solution to Equations (19) or (24). In other words, for this particular case, the final solution for h is obtained by taking step 1 first, then step 2 (using h^{up} resulted from Equation (19) as h^n in Equation (24)) and finally step 4 (using h^{up} resulted from Equation (24) as in Equation (16) for the final solution, h^{n+1}).

5. GSHAW5

The program GSHAW5, developed by the first author, is written in the object-oriented programming language DELPHI 5 and it is user friendly. The surface component of the model was applied in previous studies [7, 20, 21]. The main features of the model are

(a) Suitability for simulation of shallow surface and saturated subsurface flow interaction
(b) Suitability for different types of surface flow including continuous and discontinuous flow, steady and unsteady flow, subcritical and supercritical flow.
(c) It has the ability to handle different surface boundary conditions. The boundary conditions available in the program include rating curves, time-dependent discharge boundaries, given discharge and or water depth and closed or open boundaries.
(d) Suitability for flow in initially dry areas and drying and wetting flow conditions.

6. TEST CASES AND RESULTS

GSHAW5 has been tested for a number of hypothetical cases, which are explained below. In all applications, the specific yield values are set to unity in order to easily check the mass balance at the end of each computation. However, in reality, depending on the type of material this value changes, i.e. 0.01 for clay to 0.46 for sand (medium size) [10]. The hydraulic conductivity values are also artificially produced but they are within the range of realistic values [9].

Test 1: A computational domain, 20 m long and 1 m wide, is divided into 20 cells, each of which has a 1×1 m size. The ground elevation (the aquifer thickness) is 2 m. Initially, groundwater head is assumed to have a constant value of 1.5 m everywhere (which is 0.5 m below the ground level). The surface water depth is 1 m everywhere. Figure 4 shows the initial conditions described above. The boundaries for both surface and groundwater are assumed to be closed. Artificial hydraulic conductivity values are chosen to be 1×10^{-5} m/s. This test is frictionless and there is no bottom slope.

It can be anticipated that after a sufficiently long simulation, flow in the domain should reach the equilibrium condition, i.e. 2.5 m groundwater head and 0.5 m water depth everywhere since mass should be preserved.

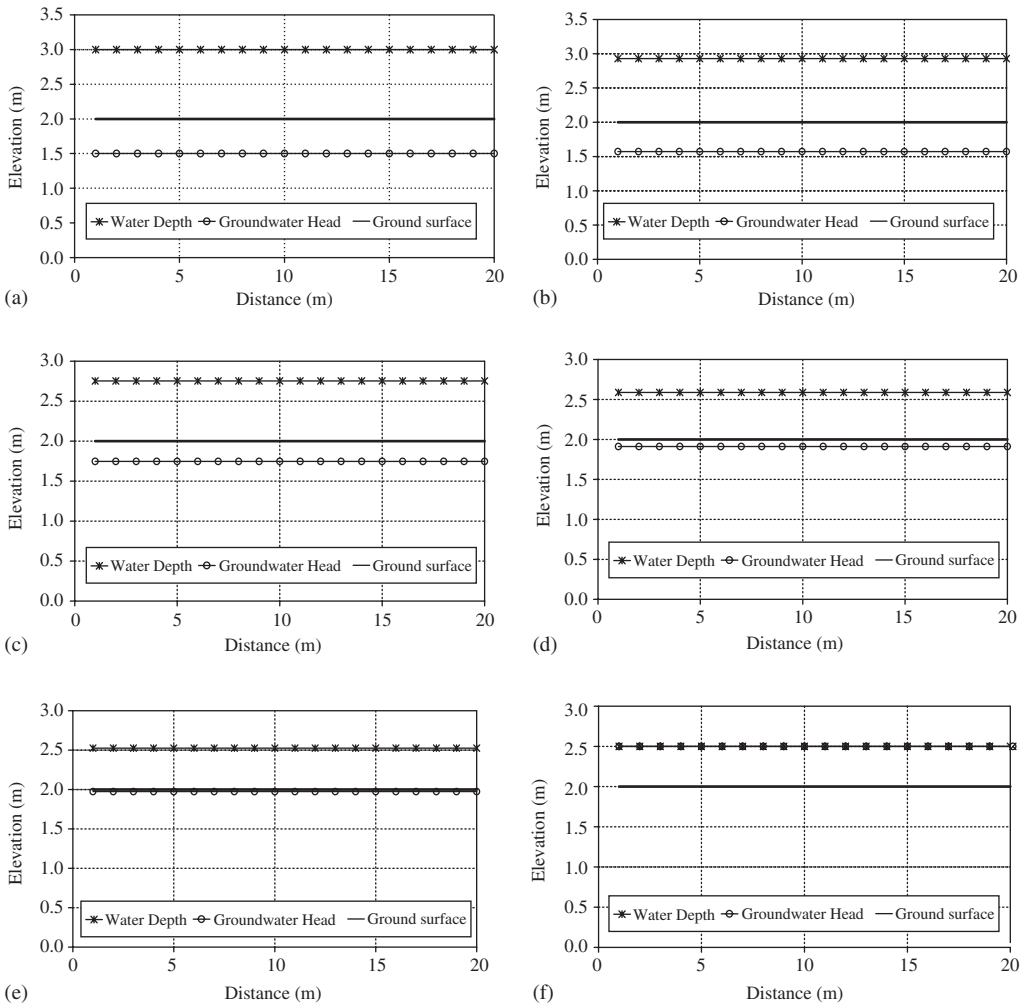

Figure 4. Groundwater and surface water integration processes for Test 1: (a) initial; (b) 10 000 s; (c) 40 000 s; (d) 80 000 s; (e) 100 000 s; and (f) 110 000 s.

Results obtained show that after 110 000 s the equilibrium flow condition is obtained with no loss or excess of water (Figure 4).

Test 2: In this test the same computational domain and grid are used as in Test 1. The computational domain is divided into two regions: left and right of the middle of the domain (Figure 5(a)). On the left side, the surface water depth is initially equal to 2 m, while on the right side it is 1 m, providing a rapidly varying flow on the surface. On the right side, the groundwater head is above the ground and is equal to $h + Z = 4$ m. On the left side, it is below the ground level and equal to 1.5 m. Boundary conditions are selected as closed for both surface and groundwater. Under these conditions, it is expected that the mass will be redistributed. The water depth on the surface will become 1.25 m and will remain constant. The groundwater head is expected to be equal to 3.25 m (2+1.25 m).

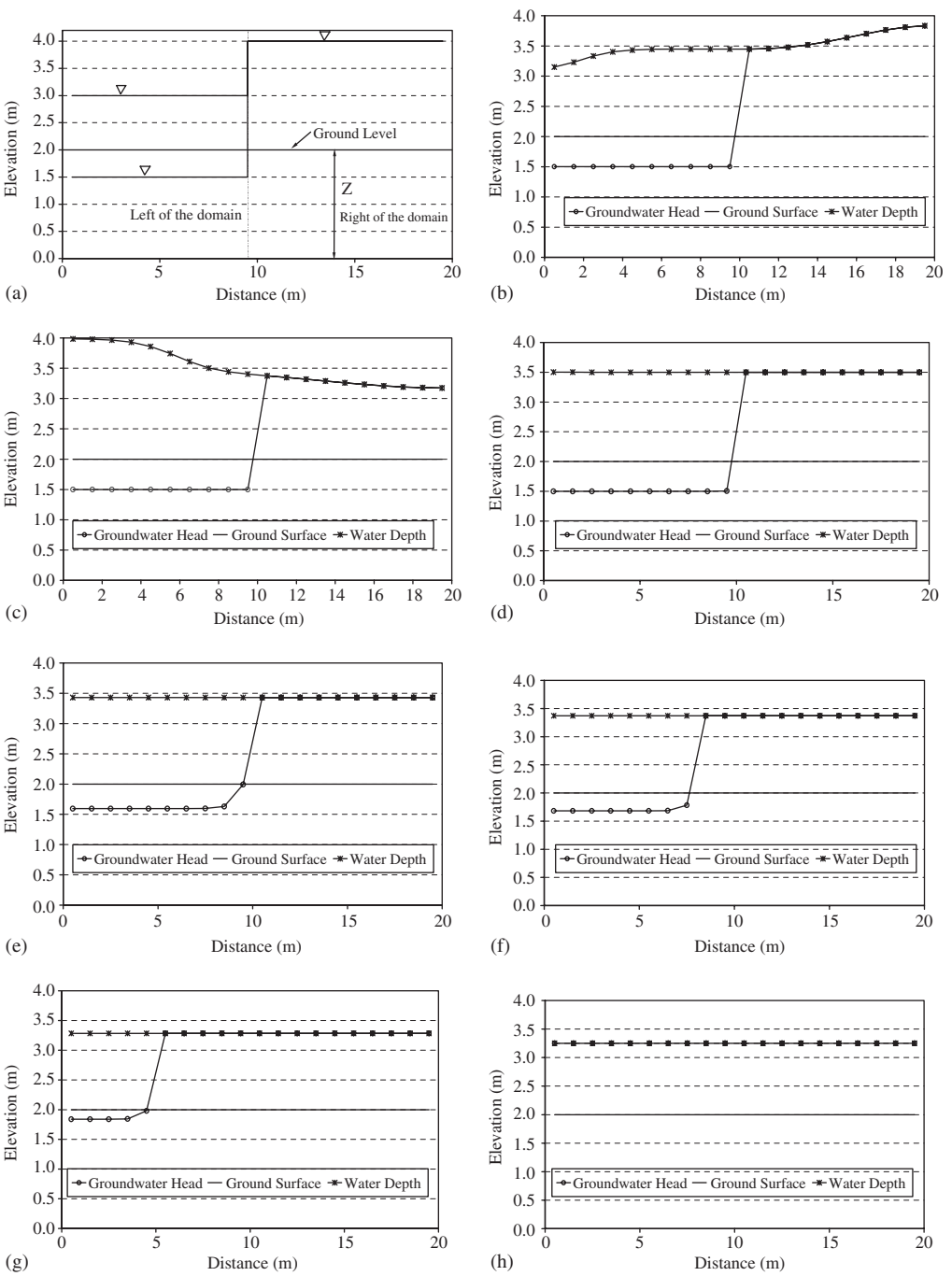

Figure 5. Groundwater and surface water integration processes for Test 2: (a) initial; (b) 2 s; (c) 4 s; (d) 60 s; (e) 10 000 s; (f) 20 000 s; (g) 40 000 s; and (h) 60 000 s.

As seen in Figures 5(b) and (c), there is a rapid change on the surface water after 2 and 4 s, respectively, due to the large initial difference in water depths. The surface water has fluctuated between the closed boundaries at both ends of the domain for 60 s. However, during that period there is no movement of the groundwater head as the leakage rate is very low and, in such a short period, there is almost no groundwater lateral flow. When the simulation time reaches 60 s, the water surface almost reaches a steady state condition, whilst there is still no significant change in the groundwater head. At a time of 10 000 s, there is a considerable drop on the surface due to infiltration on the left-hand side of the domain. The groundwater head increases due to the infiltration and the lateral flow caused by the head differences, particularly in the middle of the domain. Similar but more significant changes are seen at times 20 000 s and 40 000 s. Finally, the expected equilibrium condition is obtained at 60 000 s.

This test is used to demonstrate groundwater flow, due to the head differences and infiltration, and surface flux due to water depth differences. The results show that the expected flux occurred and that total mass was preserved. The test also demonstrates that the splitting technique and time coupling of surface and groundwater computation have not produced inaccuracies.

Test 3: A 70 m long channel is divided into 70 cells, each of which has a 1×1 m size. Between 0 and 40 m, the channel has a downward slope of 0.1 from the upstream, followed by a flat bottom from 40 to 50 m and then again a downward slope of 0.2. Both upstream and downstream boundaries are closed. The groundwater boundaries are also closed. Artificial hydraulic conductivity values are chosen to be 1×10^{-5} m/s. Manning's friction coefficient is taken to be 0.02. Initially, surface water elevation is equal to 8 m everywhere. The groundwater head between 0 and 40 m is equal to 4 m, while between 40 and 70 m it is effectively equal to surface water elevation (8 m). Initial conditions are shown in Figure 6. It is expected the surface water will feed the groundwater. The surface water will gradually reduce whereas the groundwater head values between 0 and 40 m will increase. There should not be any loss or excess of water from the system as all boundaries are closed.

The surface water level and groundwater head values at different times are plotted in Figure 6. Before reaching the equilibrium condition, the groundwater head between 0 and 40 m increases due to the infiltration and the lateral flow caused by the head differences. The lateral groundwater movement occurs towards the upstream direction, whereas the infiltration occurs in the vertical direction. The surface water level reduces and the surface cells upstream start drying. Finally, the equilibrium condition occurs at 6.86 m from the datum (0 m). The total initial volume of water is 480 m^3 and the total volume of water at the equilibrium is also equal to 480 m^3 Mass is well preserved.

This test is set up in order to demonstrate that the model can handle drying flow processes and also flow on variable bottom topography. Following Brufau *et al.* [14] the slope modification procedure is also introduced in the model in case the 'stopping' flow condition occurs, which result in mass errors. The stopping flow condition occurs when the sum of water depth and the ground elevation in the centre of the cell under consideration exceeds the sum of water depth and ground elevation in the centre of the neighbouring cell (other side of the cell interface). If this case happens, then the slope at that interface is modified and the quantity $(z_R - z_L)$ is replaced by $-(h_R - h_L)$. However, it should be noted that this modification works quite well for steady flow cases but for unsteady flow cases the velocities at the cell interface are reduced to zero, which can produce mass errors in unsteady flow conditions [14].

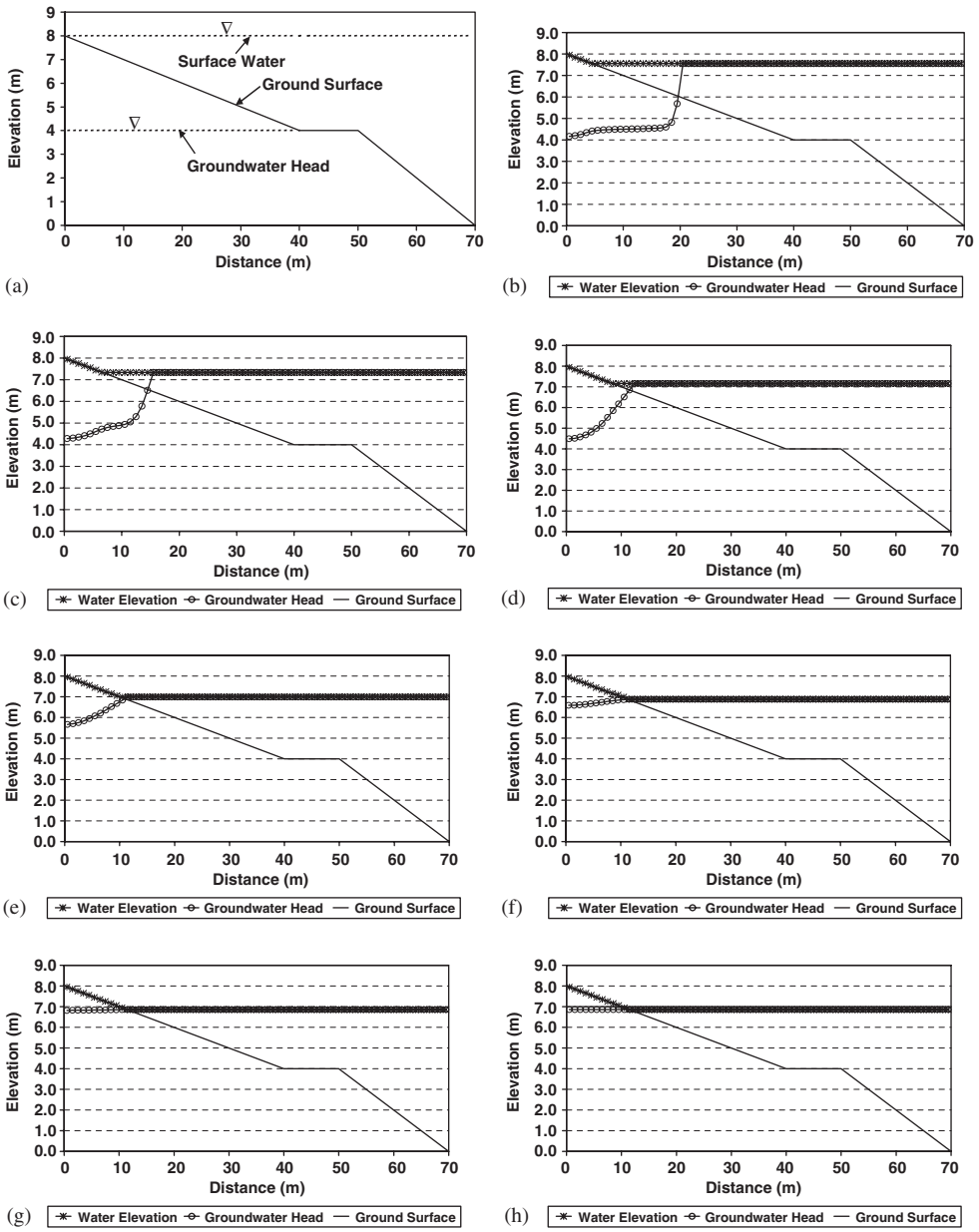

Figure 6. Groundwater and surface water integration processes for Test 3: (a) initial; (b) 100 000 s; (c) 200 000 s; (d) 400 000 s; (e) 1 000 000 s; (f) 1 800 000 s; (g) 300 0000 s; and (h) 6 800 000 s.

Test 4: This test is a 2-D application of the model. The domain is 100 m long and 40 m wide. It is divided into 50×20 cells, each 2×2 m in size. At a point 10 m, a waterproof barrier is placed in a vertical direction so the surface water boundary at that point is closed

and groundwater movement is allowed only under the barrier. Manning's friction coefficient is taken to be 0.02 and the hydraulic conductivity value is set to be 2×10^{-5} m/s. The computational domain, with initial flow conditions, is illustrated in Figure 7. From the upstream boundary to 10 m into the domain, the ground level is 10 m and the bottom is flat. In this part, there is no surface water but the groundwater head is equal to 3 m. Between 10 and 100 m a bottom slope of 0.001 in both x and y directions is applied. The groundwater head is constant between 10 and 100 m and is equal to 1.87 m. Between 10 and 90 m the water level is equal to 2.1 m and between 90 and 100 m a water depth of 4 m is applied. Figures 8(a)–(c) show the cross-sectional views of the set-up. It can be seen that this set-up produces varying ground and water levels in both x and y directions. All outside boundaries both for the surface water and groundwater, are closed so that the mass balance can be checked. There should be no excess or loss of mass.

Under these flow conditions, the following flow motion is expected; the surface water between 90 and 100 m on the right-hand side of the domain propagates fast to the left and when it reaches the barrier it is reflected back. This produces a fluctuating water surface and the surface flow motion continues until it reaches the equilibrium stage. During this movement and also after the equilibrium on the surface water, there will be a certain amount of surface water which gradually joins the groundwater by infiltration until the groundwater head reaches the ground level. In terms of groundwater motion, a certain amount of groundwater from the left side of the barrier will gradually pass under the barrier and the groundwater head on

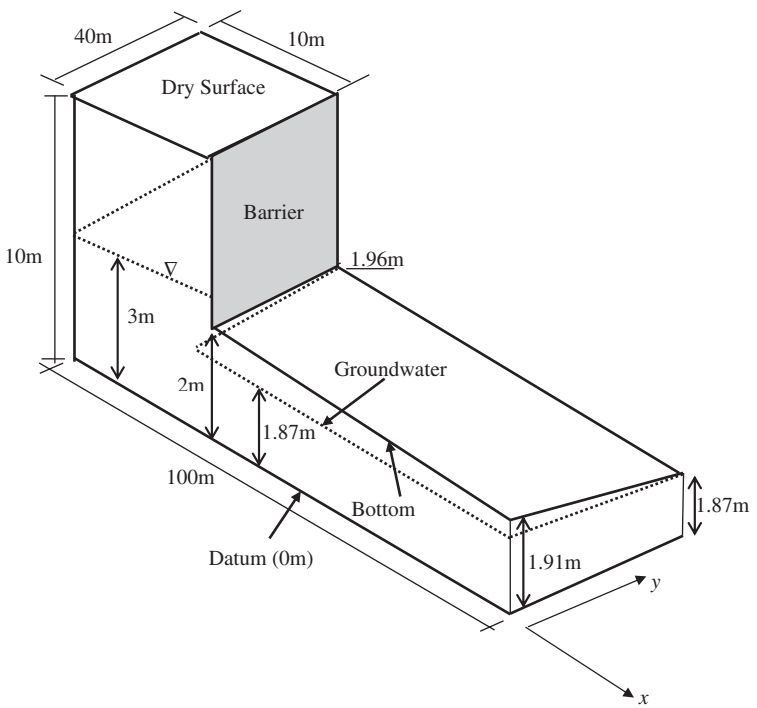

Figure 7. Computational domain and initial groundwater flow condition for Test 4.

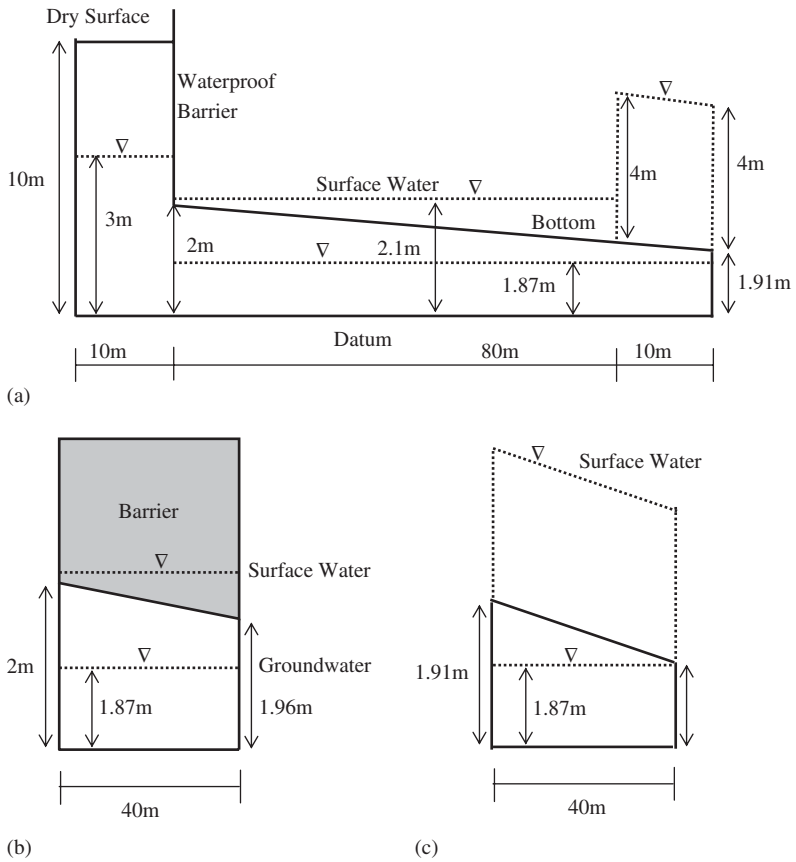

Figure 8. Cross-sectional views of initial flow condition and computational domain for Test 4: (a) $(x, y) = (0, 0) - (100\,\mathrm{m}, 0)$; (b) $(x, y) = (10\,\mathrm{m}, 0) - (10\,\mathrm{m}, 40\,\mathrm{m})$; and (c) $(x, y) = (100\,\mathrm{m}, 0) - (100\,\mathrm{m}, 40\,\mathrm{m})$.

the right-hand side of the barrier raises. The rate of increase on the groundwater head on the right-hand side of the barrier depends on the vertical infiltration rate and the horizontal groundwater flow rate from the right-hand side of the barrier. This process will continue until the overall equilibrium condition (static flow in the domain) is achieved.

The results are illustrated in Figures 9–11. Figures 9(a)–(c) show the water depth profiles at 10, 200 and 2000 s, respectively. The initially unbalanced water on the surface moves to the barrier first and then turns back and propagates towards downstream. This movement almost stops at 2000 s as shown in Figure 9(c). During the surface water motion, the infiltration from surface to ground also takes place but the infiltration rate is very low. The horizontal groundwater fluxes are also low compared to those of the surface water. Therefore, the groundwater head values change gradually. When the groundwater reaches the ground level, the groundwater head (the pressure head) becomes $h + Z$ as explained in Section 4, see Case B. As expected, the occurrence of Case B starts from the lowest ground level and moves

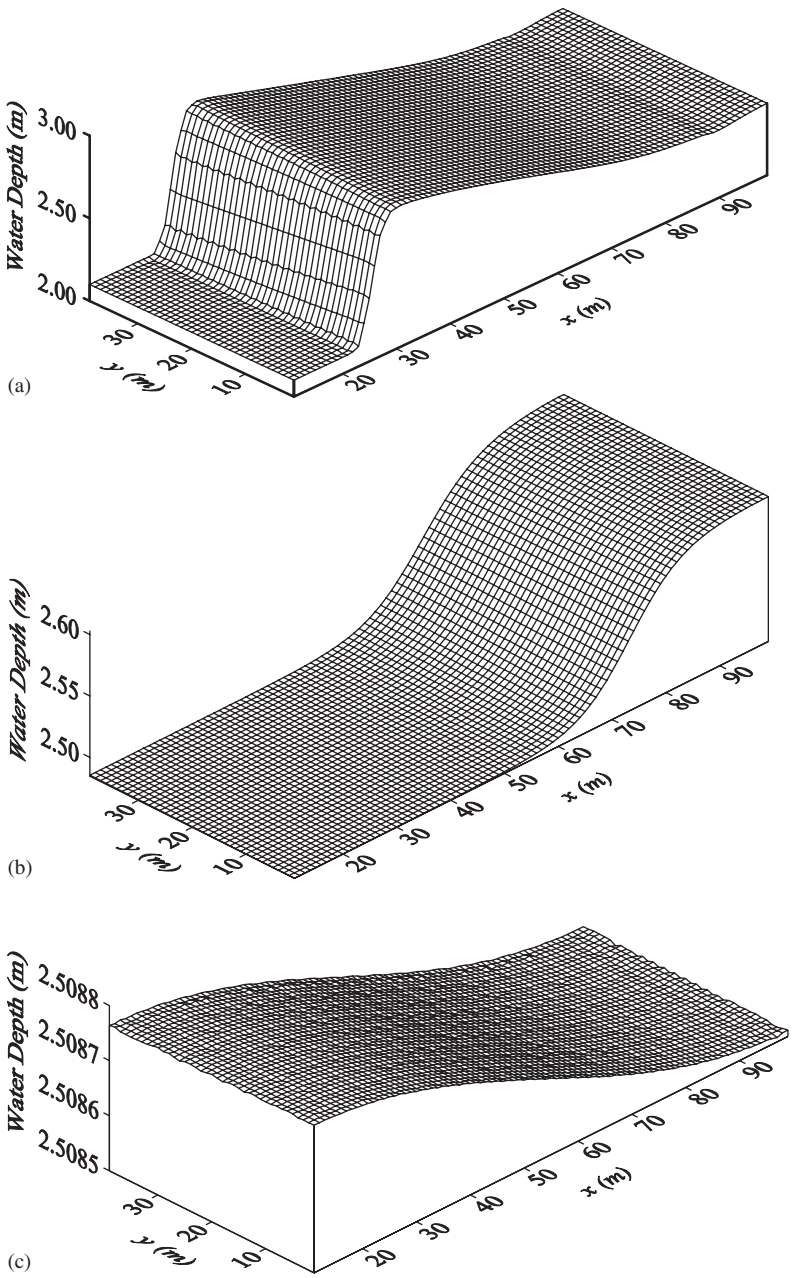

Figure 9. Surface water depth profiles after the barrier for Test 4 at: (a) 10 s; (b) 200 s; and (c) 2000 s.

to highest point, as shown in Figures 10(a)–(c). The groundwater head on the left side of the barrier decreases (starts at 3 m and reaches $\cong$ 2.51 m) and overall equilibrium condition occurs almost at 10.8×10^6 s as demonstrated in Figure 11. Initially, total volume of water

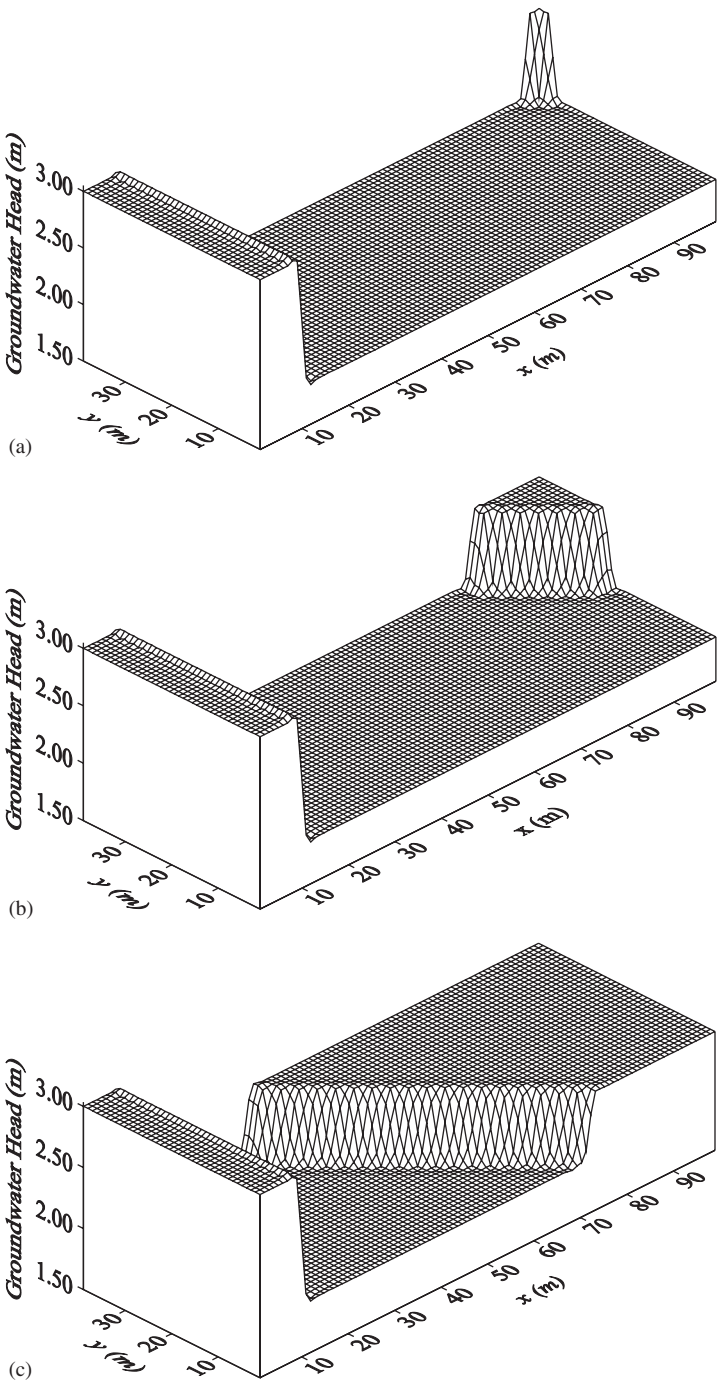

Figure 10. Groundwater head $(h + z)$ profiles for Test 4 at: (a) 200 s; (b) 2000 s; and (c) 10 000 s.

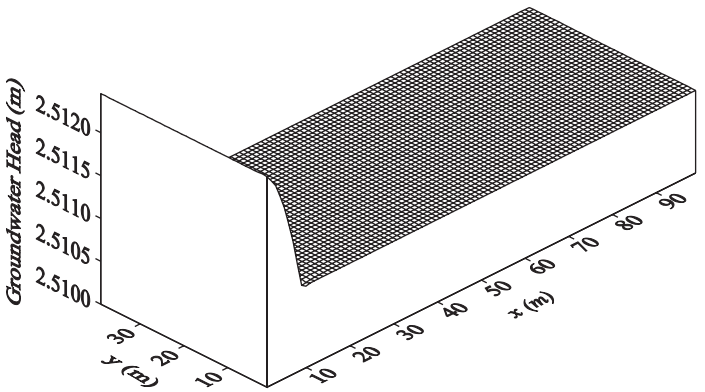

Figure 11. Groundwater head $(h + z)$ profile for Test 4 at 10.8×10^6 s.

inside the domain is 10 044 m^3 and at 10.8×10^6 s it is equal to 10044.2 m^3. Hence, the mass is again well preserved and the mass error is 0.002%. When the volume of water is divided by the number of cells multiplied by the cell area, it gives the water level inside the domain. At the equilibrium, the computed water level should be 2.511 m, which is very similar to that produced by the model, as illustrated in Figure 11.

7. CONCLUSIONS AND FURTHER WORKS

From this study, the following conclusions can be drawn.

(1) A finite volume solution for the integrated surface–saturated groundwater flow problems is provided. Surface water solution is tightly coupled with the groundwater solution so in each time step the type of interaction is checked and the suitable solution is used. The surface water solution is suitable for many flow conditions, including discontinuous flows and wetting and drying flow conditions.
(2) In all the tests provided, the hydraulic conductivity values were taken to be the same in all directions and all cell interfaces. However, the model is flexible and different values for different cell interfaces can be used. Moreover, although not shown in any example, the model can be used for the simulation of flow including rainfall as explained in Section 3.1.
(3) The splitting technique generally produces errors when it is used for the treatment of the bottom slope for the shallow water model applications [7]. Here in all applications, the errors are found to be almost none. This is probably due to the fact that the groundwater fluxes as well as the infiltration rate were very small as the time steps used were also small so the technique worked well. The presented method employs explicit solutions, which require small time steps to ensure stability, i.e. in the presented tests, time steps ranged from 0.1 to 0.5 s. In reality, groundwater fluxes are generally low and the use of small time steps ensures that the method can be applied to a wide range of surface water–groundwater interaction problems (i.e. river–aquifer interactions) and wetland management.

It is planned to continue development of this model by the introduction of a solution to multi-layers groundwater flow processes, and variable time steps between the ground and the surface flow components.

ACKNOWLEDGEMENTS

We would like to thank the Ministry of Education of Turkey and the University of Newcastle Ridley Fellowship Fund, for providing financial support for the first and the third authors of this paper during their work on this project, and Dr Geoff Parkin for helpful discussions during model development.

REFERENCES

1. Parkin G. A three-dimensional variably-saturated subsurface modelling system for river basins. *Ph.D. Thesis*, Department of Civil Engineering, University of Newcastle upon Tyne, 1996.
2. Yakirevich A, Borisov V, Sorek S. A quasi three-dimensional model for flow and transport in unsaturated and saturated zones: 1. Implementation of the quasi two-dimensional case. *Advances in Water Resources* 1998; **21**:679–689.
3. Singh V, Bhallamudi SM. Conjunctive surface-subsurface modeling of overland flow. *Advances in Water Resources* 1998; **21**:567–579.
4. Haagsma IG, Johanns RD. The interaction of groundwater and surface water studied by loosely coupled models. *IAH-ICH Volume on Shallow Groundwater Systems*. Heise Verlag: Berlin, 1996.
5. Roe PL. Approximate Riemann solvers, parameter vectors, and difference schemes. *Journal of Computational Physics* 1981; **43**:357–372.
6. Zhao DH, Shen HW, Lai JS, Tabios III GQ. Approximate Riemann solvers in FVM for 2D hydraulic shock wave problems. *Journal of Hydraulic Engineering* 1996; **122**:692–702.
7. Erduran KS, Kutija V, Hewett CJM. Performance of finite volume solutions to the shallow water equations with shock-capturing schemes. *International Journal for Numerical Methods in Fluids* 2002; **40**:1237–1273.
8. Abbott MB, Minss AW. *Computational Hydraulics* (2nd edn). Ashgate: U.S.A., 1998.
9. Bear J, Verruijt A. *Modelling Groundwater Flow and Pollution*. Kluwer Academic Publishers: Holland, 1987.
10. Anderson MP, Woessner WW. *Applied Groundwater Modelling*: *Simulation of Flow and Advective Transport*. Academic Press: U.S.A., 1992.
11. Alcrudo F, García-Navarro P. A high-resolution Godunov-type scheme in finite volumes for the 2D shallow-water equations. *International Journal for Numerical Methods in Fluids* 1993; **16**:489–505.
12. Toro EF. *Riemann Solvers and Numerical Methods for Fluid Dynamics*. Springer: Berlin, 1997.
13. Delis AI, Skeels CP, Ryrie SC. Evaluation of some approximate Riemann solvers for open channel flows. *Journal of Hydraulic Research* **38**:217–231.
14. Brufau P, Vázquez-Cendon ME, García-Navarro P. A numerical model for the flooding and drying of irregular domains. *International Journal for Numerical Methods in Fluids* 2002; **39**:247–275.
15. Hirch C. *Numerical Computation of Internal and External Flows*, vol. 2. Wiley: U.K., 1990.
16. Tan W. *Shallow Water Hydrodynamics*. Elsevier: Amsterdam, Netherlands, 1992.
17. Bermúdez A, Dervieux A, Desideri J-A, Vázquez ME. Upwind schemes for the two-dimensional shallow water equations with variable depth using unstructured meshes. *Computer Methods in Applied Mechanics and Engineering* **155**:49–72.
18. Vázquez-Cendon ME. Improved treatment of source terms in upwind schemes for the shallow water equations in channels with irregular geometry. *Journal of Computational Physics* 1999; **148**:497–526.
19. Wilson EEM, Akande O. Simulation of streamflow behavior in chalk catchments. In *Modelling River-Aquifer Interactions*, *British Hydrological Society*, *Occasional Paper No. 6*, Younger PL (ed.), University of Newcastle, Newcastle upon Tyne, U.K., 1995; 129–146.
20. Erduran KS, Kutija V. Applications of finite volume method with Osher scheme and split technique on different types of flow in channel. In *Proceedings of the International Conference on Godunov Methods*: *Theory and Applications*, Toro EF (ed.). Oxford: U.K., 1999.
21. Erduran KS, Kutija V, Hewett CJM. An investigation of a straight channel assumption for meandering channels. *Proceedings of the 4th International Conference on Hydroinformatics*, Iowa, U.S.A., 2000; 126.

